iScience

CellPress
OPEN ACCESS

Article

Integrated single-cell analyses decode the developmental landscape of the human fetal spine

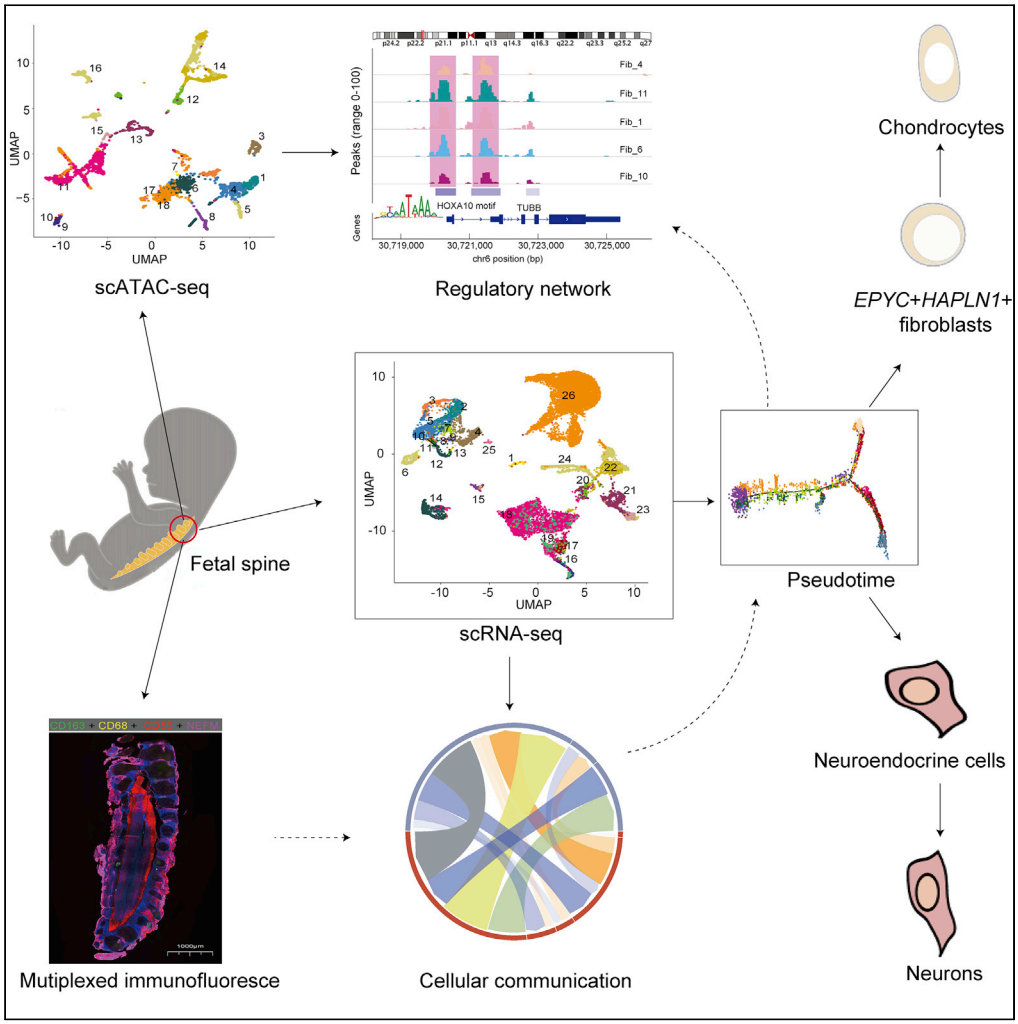

Haiyan Yu, Donge Tang, Hongwei Wu, ..., Weier Dai, Minglin Ou, Yong Dai

minglinou@glmc.edu.cn (M.O.)
daiyong22@aliyun.com (Y.D.)

Highlights

scRNA-seq and scATAC-seq analyses reveal the developmental landscape of the fetal spine

Chondrocytes may originate from *EPYC* + *HAPLN1*+ fibroblasts with stem cell characteristics

Neurons may originate from neuroendocrine cells with regulation by MEIS2

Yu et al., iScience *25*, 104679
July 15, 2022
https://doi.org/10.1016/j.isci.2022.104679

iScience

CellPress
OPEN ACCESS

Article

Integrated single-cell analyses decode the developmental landscape of the human fetal spine

Haiyan Yu,[1,2,9] Donge Tang,[1,9] Hongwei Wu,[1] Chunhong Li,[1] Yongping Lu,[1,3] Fang He,[4] Xiaogang Zhang,[4] Yane Yang,[5] Wei Shi,[6] Wenlong Hu,[1] Zhipeng Zeng,[1] Weier Dai,[7] Minglin Ou,[8,*] and Yong Dai[1,10,*]

SUMMARY

The spine has essential roles in supporting body weight, and passaging the neural elements between the body and the brain. In this study, we used integrated single-cell RNA sequencing and single-cell transposase-accessible chromatin sequencing analyses to reveal the cellular heterogeneity, lineage, and transcriptional regulatory network of the developing human spine. We found that *EPYC* + *HAPLN1*+ fibroblasts with stem cell characteristics could differentiate into chondrocytes by highly expressing the chondrogenic markers *SOX9* and *MATN4*. Neurons could originate from neuroendocrine cells, and MEIS2 may be an essential transcription factor that promotes spinal neural progenitor cells to selectively differentiate into neurons during early gestation. Furthermore, the interaction of NRP2_SEMA3C and CD74_APP between macrophages and neurons may be essential for spinal cord development. Our integrated map provides a blueprint for understanding human spine development in the early and midgestational stages at single-cell resolution and offers a tool for investigating related diseases.

INTRODUCTION

The spine facilitates neurotransmission and protects the body from trauma and excessive strain that may occur during physical movement (Galbusera and Wilke, 2018). Defects in the early stages of spine development may lead to neural tube defects and vertebrae and rib deformities (Weiss and Moramarco, 2016) (Saavedra et al., 2018). The human spine originates during the third and fourth weeks of gestation, when the blastula develops into the gastrula and is composed of the ectoderm, mesoderm, and endoderm (Slack, 2005). Previous studies on spine development have provided insights into the differentiation and development of mesodermal progenitor cells and neuroectodermal progenitor cells (Galbusera and Bassani, 2019) (Kaplan et al., 2005). However, detailed knowledge of the cell types and their developmental features in the early and midgestational stages is still lacking, especially regarding the heterogeneity of fibroblasts, chondrocytes, and neurons and their immune environment. In this study, we used integrated single-cell RNA sequencing (scRNA-seq) and single-cell transposase-accessible chromatin sequencing (scATAC-seq) to systematically dissect the cellular features and molecular regulation of the human fetal spine and reveal the landscape of transcriptomic regulation during the early stages of fetal spine development.

RESULTS

Integrated cellular landscape of the human fetal spine at the single-cell level

To investigate the developmental trajectory of fetal spines, we performed scRNA-seq and scATAC-seq of spine samples from aborted fetal tissues between 8 and 17 gestational weeks (Figures 1A and S1A, and Table S1). With scRNA-seq, we captured 16,746 cells and identified 26 cell types, including hematopoietic lineage cells, progenitor cells, neurocytes, osteoblasts, and stromal cells (Figures 1B, S1B, and S1C, Tables S2–S4). With scATAC-seq, we captured 4,848 cells and identified 18 cell types (Figures 1C and S1D, Tables S5 and S6). Overall, the cell types identified by scRNA-seq and scATAC-seq were consistent, except for eight cell types occurring at low percentages. This is possibly due to the lower number of cells captured by scATAC-seq (Tables S4 and S6).

In the fourth week of gestation, the neural tube consisting of neuroectodermal progenitor cells develops (Galbusera and Bassani, 2019), and annulus fibrosus derived from mesoderm cells appears, leading to

[1]Clinical Medical Research Center, The Second Clinical Medical College of Jinan University, The First Affiliated Hospital of Southern University of Science and Technology, Shenzhen People's Hospital, Shenzhen, Guangdong 518020, P.R. China

[2]Department of Pharmacy, Shenzhen Pingshan District People's Hospital, Pingshan General Hospital of Southern Medical University, Shenzhen, Guangdong 518118, P.R. China

[3]Institute of Nephrology and Blood Purification, the First Affiliated Hospital of Jinan University, Jinan University, Guangzhou 510632, China

[4]Singleron Biotechnologies, Yaogu Avenue 11, Nanjing, Jiangsu, China

[5]Shenzhen Far East Women & Children Hospital, Shenzhen 518000, Guangdong, China

[6]Department of Obstetrics and Gynecology, The Second Clinical Medical College of Jinan University, The First Affiliated Hospital Southern University of Science and Technology, Shenzhen People's Hospital, Shenzhen, Guangdong 518020, P.R. China

[7]College of Natural Science, University of Texas at Austin, Austin, TX 78721, USA

[8]Central Laboratory, The Second Affiliated Hospital of Guilin Medical University, No. 212, Renmin Road, Lingui District, Guilin 541000, China

[9]These authors contributed equally

[10]Lead contact

*Correspondence: minglinou@glmc.edu.cn (M.O.), daiyong22@aliyun.com (Y.D.)

https://doi.org/10.1016/j.isci.2022.104679

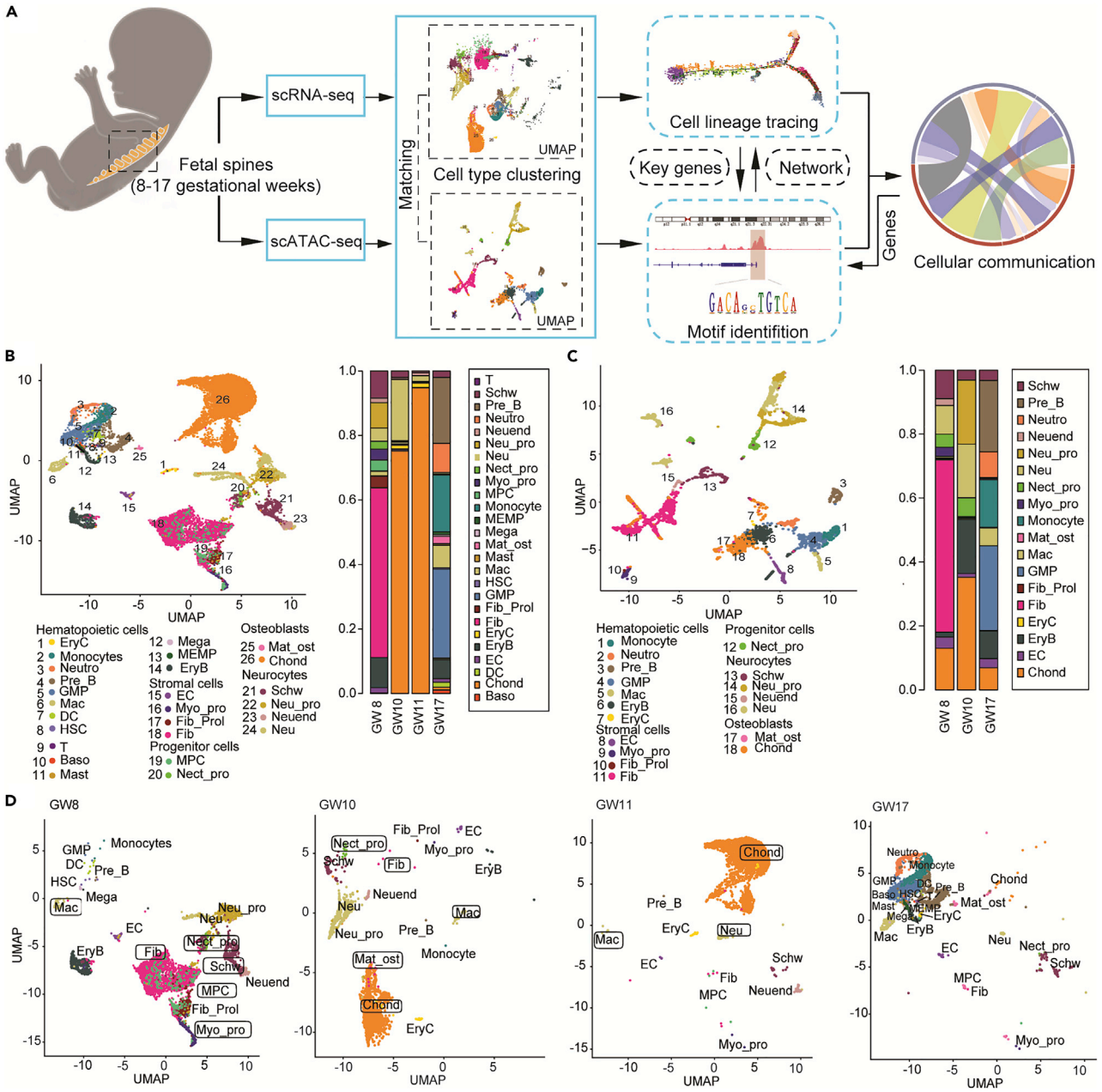

Figure 1. Integrated single-cell landscape of the human fetal spine

(A) The workflow of single-cell sequencing data production and analysis.

(B) Single-cell transcriptome landscape of the human fetal spine and the percentage of all cell types distributed in each sample at different stages of pregnancy.

(C) Single-cell open chromatin profile of the human fetal spine and the percentage of all cell types distributed in each sample at different stages of pregnancy.

(D) UMAP visualization of the cell type changes occurring in each developmental stage according to clusters in (B).

vertebral bodies, ligaments, and endplates (Lawson and Harfe, 2017) (Nolting et al., 1998). Consistently, we observed that neurocytes and fibroblasts all existed in the eighth gestational week. Fibroblasts are the dominant cell type of fetal spines, aligning well with their role in osteogenesis promotion (Zhang et al., 2017b). The nucleus pulposus develops from the notochord as early as the third and fourth weeks of gestation (Alkhatib et al., 2018), and every future vertebra will begin to ossify between the ninth and fourteenth weeks (Szpinda et al., 2013). Our results show that chondrocytes appeared in the 10th gestational week at a

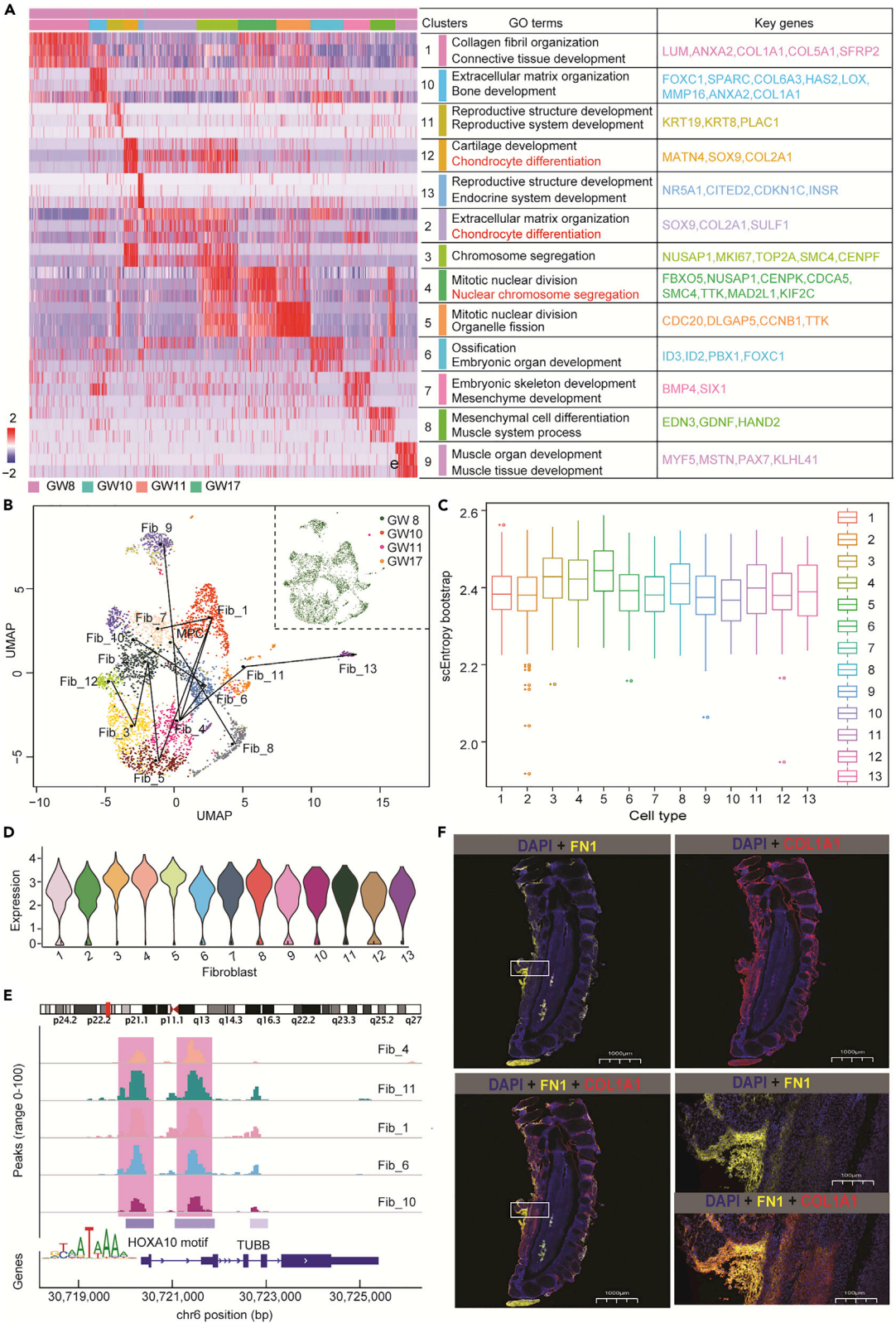

Clusters	GO terms	Key genes
1	Collagen fibril organization Connective tissue development	LUM,ANXA2,COL1A1,COL5A1,SFRP2
10	Extracellular matrix organization Bone development	FOXC1,SPARC,COL6A3,HAS2,LOX, MMP16,ANXA2,COL1A1
11	Reproductive structure development Reproductive system development	KRT19,KRT8,PLAC1
12	Cartilage development Chondrocyte differentiation	MATN4,SOX9,COL2A1
13	Reproductive structure development Endocrine system development	NR5A1,CITED2,CDKN1C,INSR
2	Extracellular matrix organization Chondrocyte differentiation	SOX9,COL2A1,SULF1
3	Chromosome segregation	NUSAP1,MKI67,TOP2A,SMC4,CENPF
4	Mitotic nuclear division Nuclear chromosome segregation	FBXO5,NUSAP1,CENPK,CDCA5, SMC4,TTK,MAD2L1,KIF2C
5	Mitotic nuclear division Organelle fission	CDC20,DLGAP5,CCNB1,TTK
6	Ossification Embryonic organ development	ID3,ID2,PBX1,FOXC1
7	Embryonic skeleton development Mesenchyme development	BMP4,SIX1
8	Mesenchymal cell differentiation Muscle system process	EDN3,GDNF,HAND2
9	Muscle organ development Muscle tissue development	MYF5,MSTN,PAX7,KLHL41

Figure 2. Developmental tracking of fibroblasts

(A) Enriched genes and pathways in each subcluster to display fibroblast heterogeneity by GSVA.

(B) Trajectory between mesodermal progenitor cells and fibroblast subclusters to show the potential differentiation directions; the beginning of the trajectory is indicated by the green dot standing for mesodermal progenitor cells (MPC).

(C) SLICE analysis of fibroblasts across different clusters to evaluate cell stemness. SLICE: determining cell differentiation and lineage based on single-cell entropy. The higher the entropy is, the greater the differentiation potential.

(D) Violin plots showing the expression of *TUBB* in fibroblast subclusters.

(E) scATAC-seq profile of *HOXA10* downstream genes and the HOXA10 motif.

(F) Immunofluorescence staining of FN1 and COLIA1 in the spine at 8 weeks of gestation. The lengths of the representative and enlarged scale bars are 1000 and 100 μm, respectively.

very high proportion in the 10th and 11th gestational weeks (Figure 1D), which correlates well with previously published literature (Szpinda et al., 2013). In week 17, hematopoietic lineage cells became dominant, consistent with the literature that hematopoietic cells are generated and propagate during the 11th and 20th weeks of gestation, respectively (Holt and Jones, 2000) (Figure 1D). Notably, macrophages, a type of hematopoietic cell, were already detected in the eighth gestational week. This result may indicate that early-stage macrophages migrate from organs such as the liver instead of from the bone marrow (Popescu et al., 2019).

Fibroblast heterogeneity and developmental tracking

To elucidate fibroblast cellular and functional heterogeneity, we performed unsupervised clustering and identified 13 subclusters of cells (Figures 2A, S2A, and S2C). As a result, cells in cluster 4 enriched for *HIST1H1A* and with minimal detection of *COL2A1* (Fib_4) were defined as *HIST1H1A* + *COL2A1*– fibroblasts (Figure S2C). Similarly, cells in cluster 12 were defined as *EPYC* + *HAPLN1*+ fibroblasts (Fib_12) because they highly expressed both *EPYC* and *HAPLN1* (Figure S2C). By gene set variation analysis (GSVA) of differentially expressed genes among the clusters, we found that *NEB* + *PAX7*+ fibroblasts (Fib_9) were enriched for genes involved in muscle organ development (Figure 2C). *PAX1*+*HOXA7*+ fibroblasts (Fib_2) and *EPYC* + *HAPLN1*+ fibroblasts (Fib_12) were enriched for genes related to the chondrocyte differentiation pathway, such as *SOX9* and *COL2A1* (Figure 2A). *HIST1H1A* + *COL2A1*– fibroblasts (Fib_4) were likely active in nuclear chromosome segregation and enriched for *FBX O 5* and *NUSAP1* (Figure 2A). These results confirm that different subtypes of spinal fibroblasts might have specific roles in forming bone and protecting the spinal cord (Zhang et al., 2017b).

To gain deeper insights into the fibroblast development process, we performed trajectory analysis with the R package slingshot. Because fibroblasts are believed to develop from mesodermal progenitor cells (MPC) (Galbusera and Bassani, 2019), we revealed the potential differentiation directions between mesodermal progenitor cells and fibroblast subpopulations (Figure 2B). In detail, MPC may differentiate into *HIST1H1A* + *COL2A1*– fibroblasts (Fib_4). And the trajectory, along with *HIST1H1A* + *COL2A1*– fibroblasts (Fib_4), extended further into other subclusters with multiple developmental branches. Meanwhile, *IFI44L* + *OGN* + fibroblasts (Fib_7), *LAMA2*+*CYP1B1*+ fibroblasts (Fib_10), *EPYC* + *HAPLN1*+ fibroblasts (Fib_12), and *DLK1*+*APOA1*+ fibroblasts (Fib_13) are located at the end of the trajectory. Thus, we speculated that *HIST1H1A* + *COL2A1*– fibroblasts (Fib_4) have a higher differentiation potential than *IFI44L* + *OGN* + fibroblasts (Fib_7), *LAMA2*+*CYP1B1*+ fibroblasts (Fib_10), *EPYC* + *HAPLN1*+ fibroblasts (Fib_12), and *DLK1*+*APOA1*+ fibroblasts (Fib_13). To validate this hypothesis, we performed SLICE analysis to identify differentiation states based on single-cell entropy (scEntropy) (Guo et al., 2017). SLICE analysis showed that *HIST1H1A* + *COL2A1*– fibroblasts (Fib_4) had a high entropy score, while clusters predicted to be at the end of the trajectory, such as *EPYC* + *HAPLN1*+ fibroblasts (Fib_12) and *DLK1*+*APOA1*+ fibroblasts (Fib_13), had low entropy scores (Figure 2C), which fits well with the trajectory results. Notably, the developmental cycle trajectory showed that spinal fibroblasts finished their differentiation as early as the eighth week (Figure 2B).

To further explore genes that drive *HIST1H1A* + *COL2A1*– fibroblasts (Fib_4) to differentiate into other fibroblast subclusters, we overlapped genes in fibroblasts with an altered expression along the pseudotime and the one enriched in the eighth week, an important stage for fibroblast development. Consequently, *TUBB* enriched in GW8 was highly expressed in *HIST1H1A* + *COL2A1*– fibroblasts (Fib_4) (Figure 2D). As known, *TUBB* in fibroblasts encodes β-tubulin and is broadly expressed in the developing CNS (Sferra et al., 2020). Our result suggested that *TUBB* may be an essential gene for driving *HIST1H1A* + *COL2A1*– fibroblast (Fib_4) development in fetal spine. Interestingly, we also found an accessible

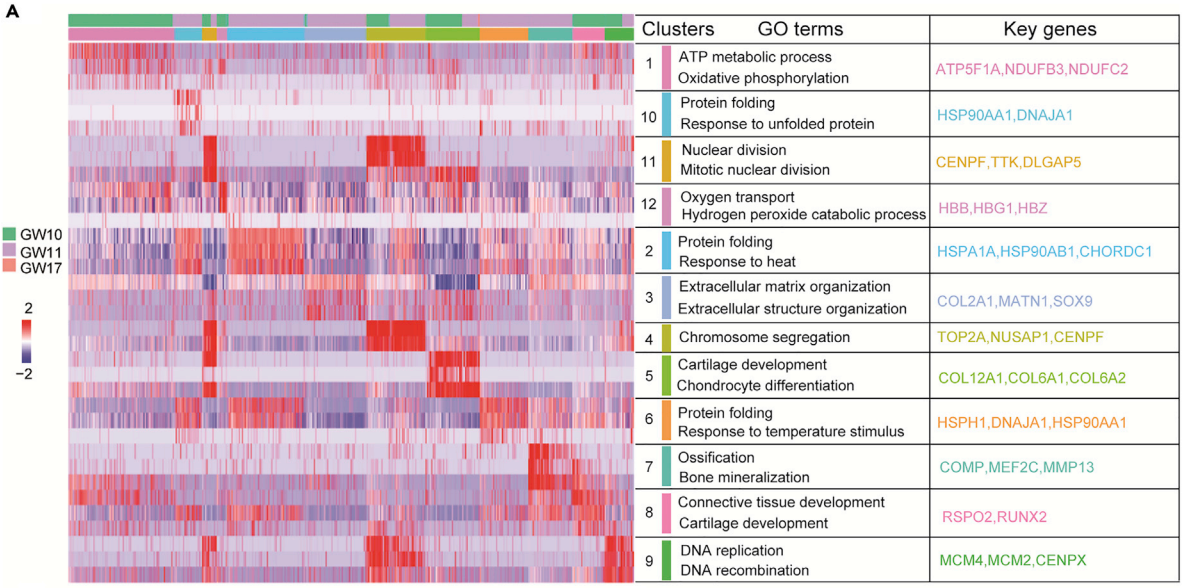

Clusters	GO terms	Key genes
1	ATP metabolic process Oxidative phosphorylation	ATP5F1A,NDUFB3,NDUFC2
10	Protein folding Response to unfolded protein	HSP90AA1,DNAJA1
11	Nuclear division Mitotic nuclear division	CENPF,TTK,DLGAP5
12	Oxygen transport Hydrogen peroxide catabolic process	HBB,HBG1,HBZ
2	Protein folding Response to heat	HSPA1A,HSP90AB1,CHORDC1
3	Extracellular matrix organization Extracellular structure organization	COL2A1,MATN1,SOX9
4	Chromosome segregation	TOP2A,NUSAP1,CENPF
5	Cartilage development Chondrocyte differentiation	COL12A1,COL6A1,COL6A2
6	Protein folding Response to temperature stimulus	HSPH1,DNAJA1,HSP90AA1
7	Ossification Bone mineralization	COMP,MEF2C,MMP13
8	Connective tissue development Cartilage development	RSPO2,RUNX2
9	DNA replication DNA recombination	MCM4,MCM2,CENPX

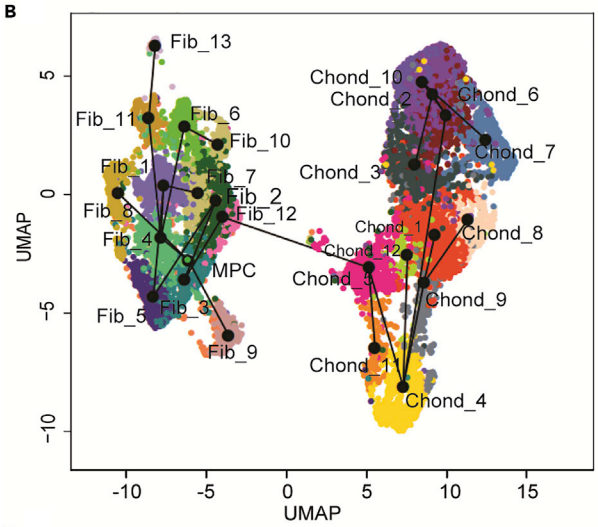

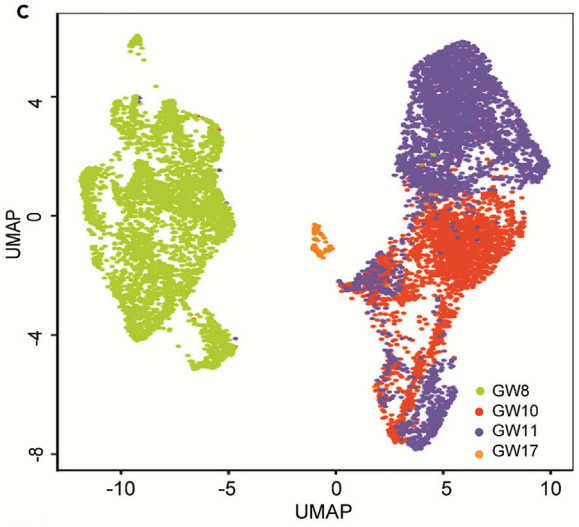

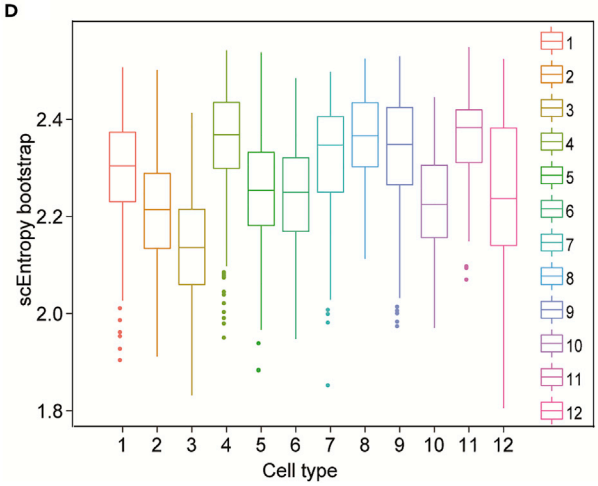

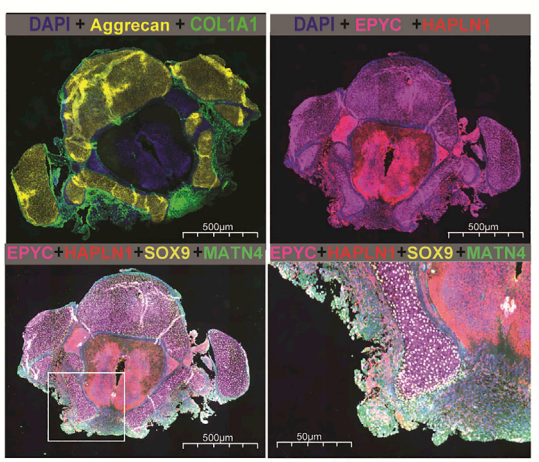

Figure 3. Developmental tracking of chondrocytes

(A) Differences in pathway activities among the 12 clusters of chondrocytes scored per cluster by GSVA.

(B and C) Trajectory between mesodermal progenitor cells and chondrocyte subclusters; the beginning of the trajectory is indicated by the green dot.

(D) SLICE analysis of chondrocytes across different clusters. SLICE: determining cell differentiation and lineage based on single-cell entropy. The higher the entropy is, the greater the differentiation potential.

(E) Immunofluorescence staining of Aggrecan, COLIA1, EPYC, HAPLN1, SOX9, and MATN4 in the spine at 8 weeks of gestation. The lengths of the representative and enlarged scale bars are 500 and 50 μm, respectively.

transcription start site (TSS) region in *TUBB* that can bind to the transcription factor HOXA10 by scATAC-seq analysis (Figure 2E). Previous studies indicated that transcription factors in the HOX family play an essential role in differentiation. As shown in our study, both *HOXA10* and its target gene *TUBB* were highly expressed in *HIST1H1A* + *COL2A1*– fibroblasts (Figure 2E). This result indicates that *TUBB* may be a critical gene to promote the differentiation of *HIST1H1A* + *COL2A1*– fibroblasts (Fib_4) to *UBE2C* + *DLGAP5*+ fibroblasts (Fib_5) by upregulating its expression through the enriched transcription factor HOXA10, thus contributing to the heterogeneity of fibroblasts and their diverse biological functions. Through immunofluorescence staining of FN1 and COLIA1, we verified the existence of fibroblasts in the eighth week and observed that fibroblasts were distributed around the spinal cord, which confirmed the heterogeneity and protective function of fibroblasts (Figures 2F, S5A, and S5B).

Cellular heterogeneity and developmental tracking of chondrocytes

Chondrocytes are critical units of the spinal column and help support body weight. We identified 12 subclusters of chondrocytes (Figures 3A and S2B, Tables S7 and S8). Most of the cells in the GW10 cycle were grouped into *TAOK1* + *HBB*– chondrocytes (Chond_1) and *ASPN* + *MKI67*– chondrocytes (Chond_5) with high expression levels of *TAOK1* and *ASPN*, respectively (Figures 3B, 3C, S2B, and S2D). The majority of cells in the GW11 cycle were divided into *HSPA1A* + *CXCL3*– chondrocytes (Chond_2) and *MT-TV* + *LGALS1*– chondrocytes (Chond_3) (Figures 3B, 3C, S2B, and S2D, Tables S9 and S10). With further functional analysis, we found that the chondrocyte differentiation pathway was highly enriched in *ASPN* + *MKI67*– chondrocytes (Chond_5) and was characterized by high expression levels of *COL12A1* and *COL6A1* (Figure 3A). Genes involved in ossification and bone mineralization as well as endochondral bone morphogenesis were enriched in *MEF2C* + *COMP* + chondrocytes (Chond_7) (Figures 3A and S2D). These results display the heterogeneity of chondrocytes.

Chondrocytes, as well as fibroblasts, develop from mesodermal progenitor cells (Galbusera and Bassani, 2019). Because fibroblasts can differentiate into chondrocytes (Hoshi et al., 1997), we performed trajectory analysis to study the relationship between mesodermal progenitor cells, fibroblast subclusters, and chondrocyte subclusters. *EPYC* + *HAPLN1*+ fibroblasts (Fib_12) seem to be critical cells that can differentiate into chondrocytes (Figure 3B). Moreover, the genes *MATN4*, *ACAN*, *COL2A1*, *COL11A1*, and *SOX9*, which are involved in chondrocyte differentiation, are enriched in *EPYC* + *HAPLN1*+ fibroblasts (Dehne et al., 2010; Komori, 2019) (Figure 2A). This result suggests that *EPYC* + *HAPLN1*+ fibroblasts have stem cell characteristics. *ASPN* + *MKI67*– chondrocytes (Chond_5) appeared at the start of the chondrocyte subcluster differentiation trajectory after the eighth week of pregnancy (Figures 3B and 3C). Besides, *MT-TV* + *LGALS1*– chondrocytes (Chond_3) and *MEF2C* + *COMP* + chondrocytes (Chond_7) located at the end of the trajectory were from the GW11 cycle (Figures 3B and 3C). The distribution of different clusters correlates well with our developmental trajectory result (Figures 1D, 3B, and 3C). SLICE analysis also suggested that *ASPN* + *MKI67*– chondrocytes (Chond_5) have a higher differentiation potential than *MT-TV* + *LGALS1*– chondrocytes (Chond_3) (Figure 3D). Additionally, *EPYC* + *HAPLN1*+ fibroblasts (Fib_12) that may develop into chondrocytes showed a lower cell number than most other fibroblast subpopulations in the eighth week. And *ASPN* + *MKI67*– chondrocytes (Chond_5) that may originate from Fib_12 showed higher cell numbers than most chondrocyte subpopulations in the 10th week (Tables S7–S10). By multiplexed immunofluorescence staining of EPYC and HAPLN1, we verify the existence of *EPYC* + *HAPLN1*+ fibroblasts (Fib_12). Further co-localization of EPYC, HAPLN1, SOX9, and MANT4 illustrates that *EPYC* + *HAPLN1*+ fibroblasts (Fib_12) may differ into chondrocytes by highly expressing SOX9 and MANT4 (Figures 3E and S5C). Notably, we hardly captured chondrocytes in the eighth week by scRNA-seq analysis, while we observed chondrocytes by immunostaining Aggrecan and MATN3 with the 8-week-old spine (Figures 3E and S5D). The possible reason may be that the spine used for immunostaining was older than the one used for scRNA-seq analysis due to sample heterogeneity. Besides, a low percentage of chondrocytes in 8-week-old spines may result in no chondrocytes detected by scRNA-seq experiments.

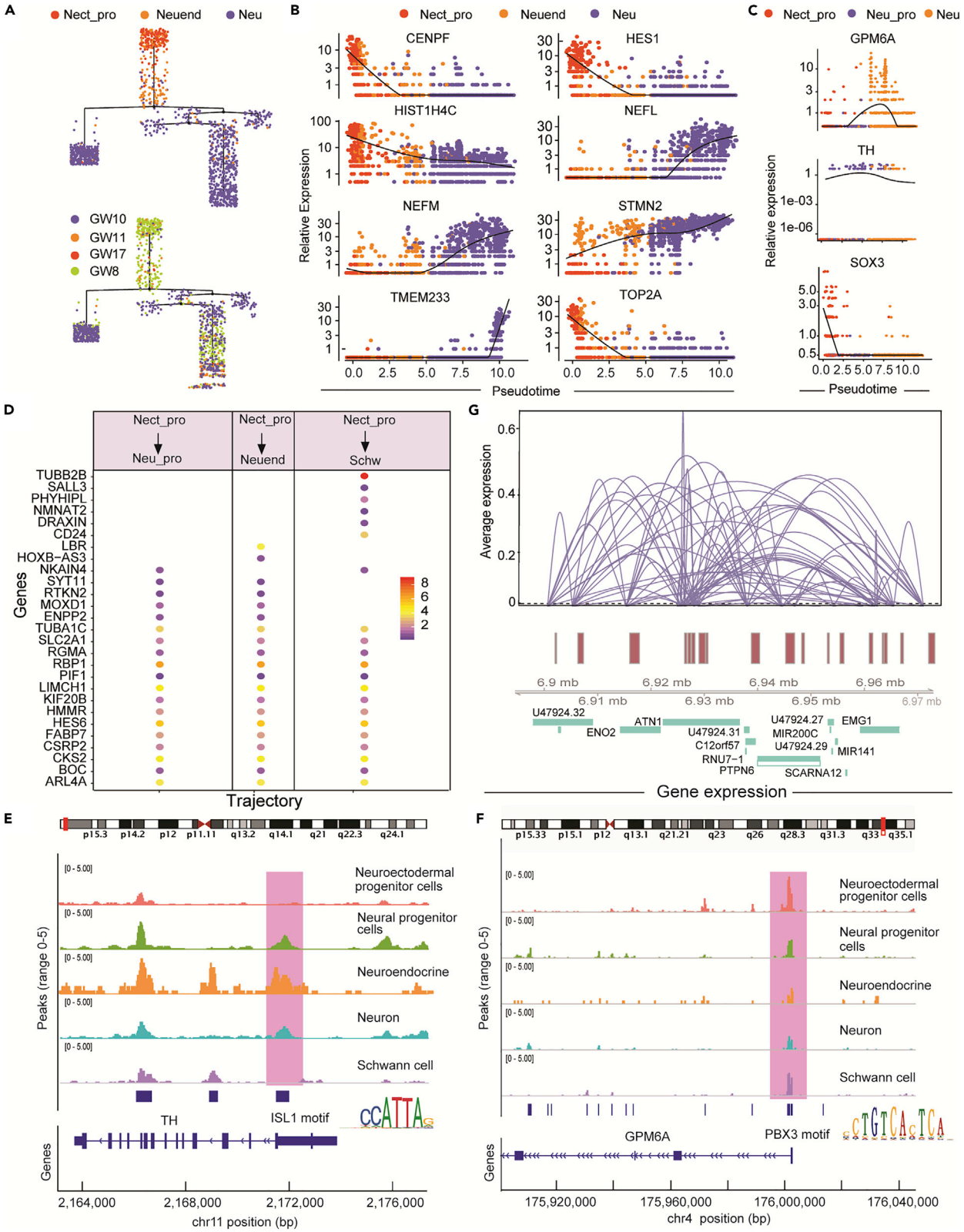
A
Nect_pro
Neuend
Neu
GW10
GW11
GW17
GW8
B
Nect_pro
Neuend
Neu
CENPF
HES1
HIST1H4C
NEFL
NEFM
STMN2
TMEM233
TOP2A
Relative Expression
Pseudotime
C
Nect_pro
Neu_pro
Neu
GPM6A
TH
SOX3
Relative expression
Pseudotime
D
Nect_pro
Neu_pro
Nect_pro
Neuend
Nect_pro
Schw
Genes
Trajectory
TUBB2B
SALL3
PHYHIPL
NMNAT2
DRAXIN
CD24
LBR
HOXB-AS3
NKAIN4
SYT11
RTKN2
MOXD1
ENPP2
TUBA1C
SLC2A1
RGMA
RBP1
PIF1
LIMCH1
KIF20B
HMMR
HES6
FABP7
CSRP2
CKS2
BOC
ARL4A
G
Average expression
Gene expression
6.9 mb
6.91 mb
6.92 mb
6.93 mb
6.94 mb
6.95 mb
6.96 mb
6.97 mb
U47924.32
ENO2
ATN1
U47924.31
C12orf57
RNU7-1
PTPN6
U47924.27
MIR200C
U47924.29
EMG1
MIR141
SCARNA12
E
Peaks (range 0-5)
Neuroectodermal progenitor cells
Neural progenitor cells
Neuroendocrine
Neuron
Schwann cell
TH
ISL1 motif
Genes
chr11 position (bp)
F
Peaks (range 0-5)
Neuroectodermal progenitor cells
Neural progenitor cells
Neuroendocrine
Neuron
Schwann cell
GPM6A
PBX3 motif
Genes
chr4 position (bp)

Figure 4. Developmental tracking of neuroectodermal progenitor cells to neurons

(A) Single-cell trajectories by Monocle analysis showing the development of neuroectodermal progenitor cells to neuroendocrine cells to neurons.

(B) Expression of known markers with pseudotime analysis.

(C) Expression of *GPM6A*, *TH*, and *SOX3* with pseudotime analysis.

(D) Average expression levels of SOX3 target genes in three developmental trajectories.

(E) ATAC-seq profile of TH downstream genes and the ISL1 motif.

(F) ATAC-seq profile of *GPM6A* downstream genes and the PBX3 motif.

(G) Line plots showing the differential coaccessibility links between the *EN O 2* regions and their surrounding regions, identified using Cicero. Peak heights (y axis) denote the coaccessibility scores.

Neurocyte developmental tracking and the potential of neuroendocrine cells to differentiate into neurons

There are five types of neurocytes (Figure 1B). To understand their relationship during development, we performed pseudotime analysis and observed three developmental trajectories that originated from neuroectodermal progenitor cells, including two reported trajectories (Kaplan et al., 2005) (Cai et al., 2017). In detail, the development from neuroectodermal progenitor cells to neural progenitor cells and then to neurons (Kaplan et al., 2005) mainly occurs during the eighth and 11th gestational weeks (Figures S3A–S3C). The developmental trajectory of neuroectodermal progenitor cells to Schwann cells (Cai et al., 2017) proceeded through the eighth to 17th gestational weeks (Figures S3D–S3F). As described in the literature, almost all endocrine cells are derived from the endoderm and neuroectoderm (Gut et al., 2015). Our results confirm that spinal neuroendocrine cells are derived from neuroectodermal progenitor cells at an early stage of pregnancy. Interestingly, we also observed that neuroendocrine cells could differentiate into neurons based on developmental trajectory analysis (Figures 4A–4C).

To further interpret this potentially new trajectory of "neuroectodermal progenitor cells to neuroendocrine cells to neurons", we found that *SOX3*, *TH*, and *GPM6A* from neuroectodermal progenitor cells, neuroendocrine cells, and neurons, respectively, seem to play a vital role in promoting the differentiation of neuroectodermal progenitor cells to neurons, which is also in agreement with the literature (Michibata et al., 2009; Wang et al., 2006) (Figure 4C). SOX3 is a conserved transcription factor labeling specific stages of human embryonic stem-cell-derived and murine neonatal and adult neural progenitors and was involved in neural stem cell maintenance (Wang et al., 2006). In total, we found 27 upregulated SOX3 target genes in the three developmental trajectories and found 14 genes, including *TUBA1C*, *SLC2A1*, and *RGMA*, which were conserved in neuroectodermal progenitor cell differentiation (Figure 4D). *HOXB-AS3* and *LBR* upregulated by SOX3 were involved in only the trajectory of "neuroectodermal progenitor cells to neuroendocrine cells to neurons", which suggested that they may be the essential genes to promote the selective differentiation of neuroectodermal progenitor cells to neuroendocrine cells (Solovei et al., 2013) (Figure 4D). Furthermore, TH in neuroendocrine cells may be a synergistic gene that promotes the final differentiation of neuroectodermal progenitor cells into neurons through its upregulation by the enriched transcription factor Islet1 (ISL1) (Liang et al., 2011) (Figure 4E). It has been reported that ISL1 played a central role in sensory neuron development linking sensory and spinal gene regulatory programs (Sun et al., 2008). Our Cicero analysis also showed high activity of the regulatory sequence of *TH*. Additionally, *GPM6A* may be an essential target gene that helps neuroendocrine cells differentiate into neurons via its upregulation by the enriched transcription factor PBX3 (Figure 4F). PBX3 was known to increase the DNA-binding/transcriptional activity of HOX proteins and regulate genes involved in development (Li et al., 2014). Moreover, our scATAC-seq data also confirmed the accessibility of the PBX3-binding site (Figure 4F). Interestingly, differentiation of neurons derived from neural progenitor cells may be driven by *ENO2*, which was highly active based on the Cicero analysis results and involved in neural differentiation (Isgrò et al., 2015) (Figures 4G and S3G).

Neuronal heterogeneity and their differentiation regulatory network in the developing human fetal spine

To study neuronal heterogeneity, we performed unsupervised clustering of 984 neurons and identified nine subclusters (Figure 5A). Through GSVA, we observed functional diversity among the nine clusters. *PMEL* + *PAPPA2*+ neurons (Neu_7), *NR2F1* + *NR2F2*+ neurons (Neu_8), and *LIX1* + *SLIT3*+ neurons (Neu_9) displayed increased expression of genes involved in neuron projection and neuron fate specification. As well known, defects in *NR2F1* are a cause of Bosch-Boonstra optic atrophy syndrome (BBOAS) (Walsh et al., 2020), indicating *NR2F1* + *NR2F2*+ neurons (Neu_8) played a vital role in neuronal development. *MAB21L2* + *TAOK1*+ neurons (Neu_1) and *ASS1* + *HES6*+ neurons (Neu_6) participate in catabolic

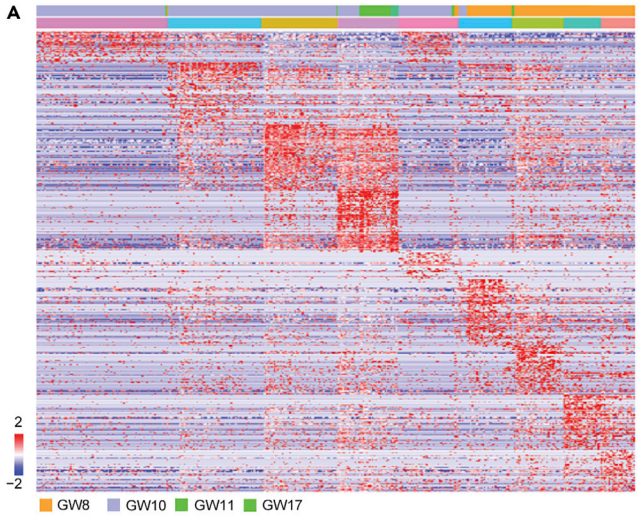

Clusters	GO terms	Key genes
1	Cartilage development Oxygen transport	COL11A1,COL2A1,MGP HBA2,HBG2,HBA1
2	Extracellular matrix organization Neuron projection regeneration	SPARC,COL2A1,FBLN1 ISL1,PTN,CTNNA1
3	Axonogenesis Regulation of neuron projection development	NTRK1,MAPT,CNTN2,FGF13 MAP1B,KIF13B
4	Action potential Axonogenesis	FGF13,SCN7A,FGF12 FGF13,NEFL,RET
5	Embryonic organ morphogenesis Spinal cord association neuron differentiation	LHX1,PAX2,GATA3,TFAP2A LHX1,ASCL1,LBX1
6	Protein localization to endoplasmic reticulum mRNA catabolic process	RPS11,RPS3,RPL37
7	Regulation of neuron projection development Neuron fate specification	NTRK3,SHOX2,NEFL NTRK3,POU4F1,TLX3
8	Developmental cell growth Neuron projection extension	SLIT2,SYT2,SEMA5A,SEMA3E
9	Neuron projection guidance Axonogenesis	SLIT2,SLIT3,LHX3,EPHA4

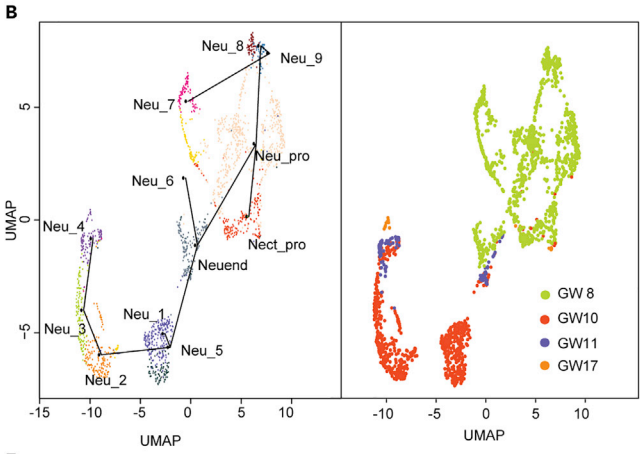

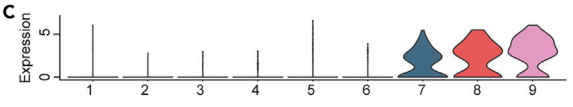

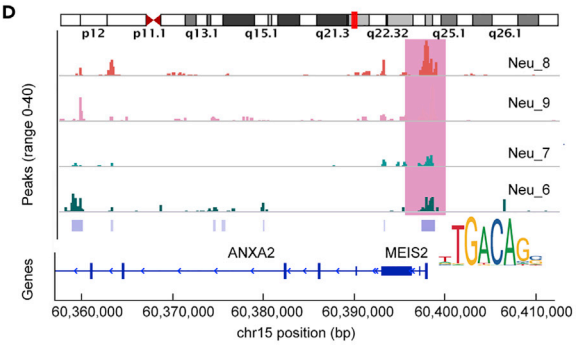

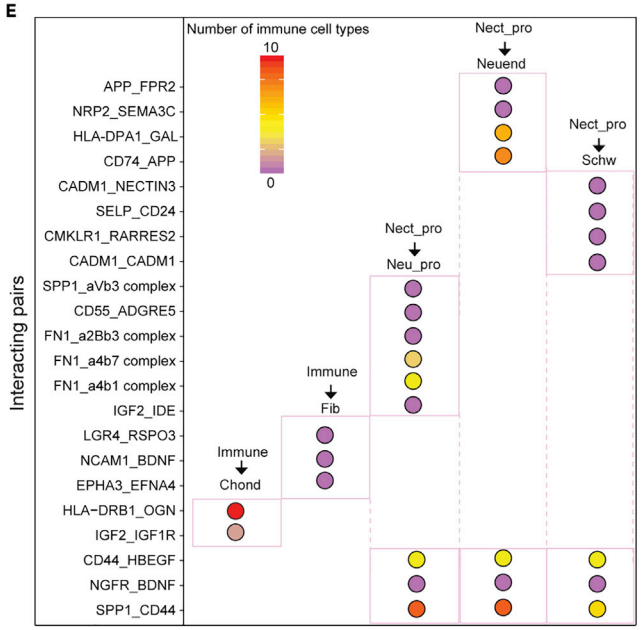

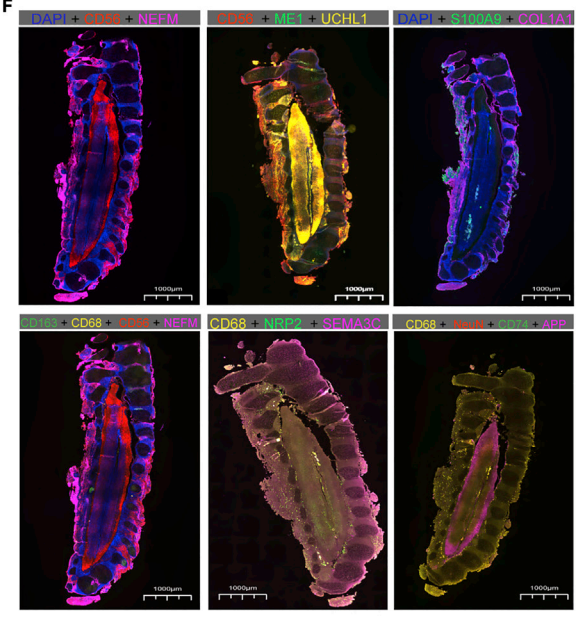

Figure 5. Neuroectodermal progenitor cell differentiation potential and cell-cell interactions in the human fetal spine

(A) Differences in pathway activities among the nine neuron clusters scored per cell by GSVA.

(B) Trajectory between neuroectodermal progenitor cells and neuron subclusters; the beginning of the trajectory is indicated by the green dot.

(C) Violin plots showing the expression of MEIS2 in neuron subclusters.

(D) ATAC-seq profile of *ANXA2* downstream genes and the *MEIS2* motif.

(E) Dotplot showing the interacting pairs of immune cells with chondrocytes, fibroblasts, and neurocytes.

(F) Immunofluorescence staining of CD56, NEFM, ME1, UCHL1, S100A9, COLIA1, CD68, CD163, SEMA3C, NRP2, NeuN, CD74, and APP in the spine at 8 weeks of gestation. The length of the representative scale bar is 1000 μm.

processes, including protein localization and oxygen transport. Notably, *TAOK1* was associated with neuronal maturation (van Woerden et al., 2021), suggesting that *MAB21L2* + *TAOK1*+ neurons (Neu_1) may be essential for neuronal maturation. *NPPA* + *CST3*+ neurons (Neu_2), *NEUROD6* + *LHX1*+ neurons (Neu_5), *PCP4* + *BCAS1*+ neurons (Neu_3), and *TMEM233* + *PIEZO2*+ neurons (Neu_4) were involved in both neuron differentiation and embryonic organ morphogenesis (Figures 5A, S3H, and S3I). Consistently, *NEUROD6* was reported to induce neuron terminal differentiation in the neonatal period of mice (Zhao et al., 2021), confirming the possible role of *NEUROD6* in embryonic spinal cord morphogenesis.

Neurons may originate from neuroendocrine cells as well as neural progenitor cells. Based on developmental trajectory analysis of neural cells, we found that *PMEL* + *PAPPA2*+ neurons (Neu_7), *NR2F1* + *NR2F2*+ neurons (Neu_8), and *LIX1* + *SLIT3*+ neurons (Neu_9) were from neural progenitor cells in the eighth gestational week, while the other neuron subclusters were from neuroendocrine cells at the late differentiation stage (8–17 weeks) (Figure 5B). A previous study performed scRNA-seq on mouse spinal cord and displayed motor neurons (MNs) were the most prominent class of neurons at early developmental stages (e9.5 and e10.5) (Delile et al., 2019). Thus, we speculated that most of the neurons in the eighth gestational week were MNs. Moreover, SLICE analysis showed low differentiation potential of *MAB21L2* + *TAOK1*+ neurons (Neu_1), which validated the developmental trajectory result that Neu_1 took the terminal position (Figure S3J). The distribution of neurons from the center of the tissue to the surrounding area for signal conduction was confirmed by immunofluorescence analysis of NEFM and CD56 in spine sections (Figure 5F).

MEIS2 is a prerequisite for neuronal differentiation through nuclear accumulation in the subventricular zone (SVZ) olfactory bulb neurogenic system (Kolb et al., 2018). Based on our results, *MEIS2* is upregulated during the development of neuroectodermal progenitor cells into neuronal cells and is significantly higher in *PMEL* + *PAPPA2*+ neurons, *NR2F1* + *NR2F2*+ neurons, and *LIX1* + *SLIT3*+ neurons. In contrast, we did not observe significant enrichment of *MEIS2* in *ASS1* + *HES6*+ neurons, *NEUROD6* + *NEUROD6*+ neurons, *MAB21L2* + *TAOK1*+ neurons, *NPPA* + *CST3*+ neurons, *PCP4* + *BCAS1*+ neurons, or *TMEM233* + *PIEZO2*+ neurons (Figures 5C and 5D). Therefore, we speculated that MEIS2 might be an essential transcription factor that drives spinal neural progenitor cells to selectively differentiate into neurons. It could also lead to the formation of *PMEL* + *PAPPA2*+ neurons, *NR2F1* + *NR2F2*+ neurons, and *LIX1* + *SLIT3*+ neurons in the early gestational stage, which regulate the differentiation of dopaminergic neurons, as mentioned above. Additionally, our scATAC-seq data show that the binding sites for MEIS2 were accessible. Furthermore, 35 target genes in *LIX1* + *SLIT3*+ neurons that could be regulated by MEIS2 were significantly upregulated, as shown by scRNA-seq analysis. For example, the target genes *ANXA2*, *ME1*, and *UCHL1* have been reported to play a role in neuronal differentiation (Naciff et al., 1996; Neuman et al., 1993; Wang et al., 2013) (Gu et al., 2018). We found that *ANXA2*, *ME1*, and *UCHL1* were upregulated by MEIS2 in *LIX1* + *SLIT3*+ neurons, indicating that ANXA2, *ME1*, and *UCHL1* likely contribute to the formation of *PMEL* + *PAPPA2*+ neurons in the spine after binding to MEIS2 (Figure 5D). Consistent with our result, immunofluorescence analysis showed co-localization of CD56, ME1, and UCHL1, indicating that ME1 and UCHL1 correlated highly with early neuron development (Figure 5F).

Development of the immune microenvironment and intercellular communication in the human fetal spine

The immune microenvironment during spine development is complex. In our study, we found that immune cells became dominant at 17 weeks of gestation. Specifically, granulocyte-monocyte progenitor cells, precursor B cells, and monocytes consist of 27.54%, 20.46%, and 17.62% of the total cells, respectively (Table S4). Notably, granulocyte-monocyte progenitor cells are the most dominant cell population, consistent with the results of a previous study in mice in which granulocyte-monocyte progenitor cells promoted immune cell differentiation and proliferation (Hérault et al., 2017). As mentioned above, we observed

macrophages as early as the eighth gestational week (Figure 1B). Its cell number first decreased gradually as the embryo developed and then propagated at 17 weeks, indicating that the immune microenvironment is formed in early gestation with circulating immune cells.

Because nonimmune cells that communicate with immune cells may be necessary to exert biological activity, we analyzed the cell-cell interaction via Cellphone DB (Efremova et al., 2020). As a result, we obtained 66 receptor-ligand pairs that may play a role in the five main differentiation trajectories mentioned above (Figures S4A and S4B). The SPP1_CD44 interaction showed high intensity in the 11th week and 17th week of gestation and was found in all three neuroectodermal progenitor differentiation processes, suggesting its role as a typical marker of neuroectodermal progenitor differentiation (Wang et al., 2020) (Figures 5E, S4D, and S4G). Both EPHA3_EFNA4 and LGR4_RSPO3 interactions, which were related to the formation of muscle stem cells in mice (Alonso-Martin et al., 2016) and differentiation of hASCs (Zhang et al., 2017a), respectively, were only observed between immune cells and fibroblast subclusters (Figure 5E). These interactions may be a crucial part of fibroblast differentiation. Moreover, our immunofluorescence analysis of S100A9 and COLIA1 on spinal sections confirmed the potential interaction of granulocyte-monocyte progenitor cells with fibroblasts (Figure 5F). IGF2_IGF1R may be vital for maintaining chondrocyte survival, as autocrine stimulation by IGF1 and IGF2 mediates chondrocyte survival *in vitro* (Loeser and Shanker, 2000) (Figure 5E).

In the neuroectodermal progenitor cell differentiation process, SEMA3C enriched in *NR2F1* + *NR2F2*+ neurons (Neu_8) interacted with NRP2 in macrophages (Figure 5E), which contributed to developmental cell growth (Figure 5A). Because NRP2_SEMA3C can promote dendritic cell migration (Sanyas et al., 2012) (Curreli et al., 2016), we speculate that this interaction could drive circulating macrophages to induce spinal neuron growth in the early gestational stage. Meanwhile, the immunofluorescence analysis of CD68, CD163, NEFM, CD56, SEMA3C, and NRP2 displayed co-existence of SEMA3C and NRP2, indicating the possible role of macrophage to promote early neuron growth through NRP2_SEMA3C interaction (Figure 5F). The MIF_CD74 interaction shows increased intensity, while that of CD200_CD200R1 shows weak intensity during the gestational stage (Figure S4C and S4E). Both interactions may be essential for macrophages to stimulate spinal neuron development (Figures 5E, S4C, and S4E). This result is consistent with the literature reporting that macrophages are necessary to establish the neurovascular network during CNS development (Chen et al., 2017) and that both MIF_CD74 and CD200_CD200R1 interactions are involved in the neuron developmental process (Hernangómez et al., 2012; Su et al., 2017). From the 8th week to the 17th week, the CD74_APP interaction between macrophages and neurons also increased, and it was involved in only the development of the "neuroectodermal progenitor cell-neuroendocrine cell-neuron" trajectory (Figures 5E, S4C, and S4F), which has been reported to be associated with the neuroinflammatory response (Castillo et al., 2017). Thus, the interaction between CD74 and APP may be a way for macrophages to drive neuron subpopulation development and diversification. Our immunofluorescence analysis confirmed the co-localization of CD68, NeuN, CD74, and APP on spinal sections, suggesting the potential interaction of CD74 with APP (Figure 5F). In the process of the "neuroectodermal progenitor cell-Schwann cell" trajectory, the SELP_CD24 interaction seems to play a role in the activation of Schwann cells (Soltész et al., 2019), and CADM1_NECTIN3 may contribute to the attachment of Schwann cells to megakaryocytes (Furuno et al., 2012). Interestingly, the interaction of CMKLR1_RARRES2, which is well known to play key roles in immune environment formation (Pachynski et al., 2019), was also observed in our study (Figure 5E). These findings emphasized the importance of immune cells in the genesis and differentiation of neurocytes in the spine.

DISCUSSION

In this study, we integrated scRNA-seq and scATAC-seq to decode the gene expression and regulatory landscape of human fetal spine development at single-cell resolution at different developmental stages. The results of the two methods were consistent and revealed similar developmental features of the central spinal cells. In detail, fibroblasts and chondrocytes, the main components involved in spinal cord protection and body weight support, were the dominant cell types in the early gestational stage and contained highly heterogeneous subpopulations. Among 13 fibroblast clusters, *HIST1H1A* + *COL2A1*– fibroblasts enriched for *TUBB* showed a high differentiation potential, suggesting that *TUBB* is a pivotal gene for promoting *HIST1H1A* + *COL2A1*– fibroblast differentiation and helping construct the diverse stromal environment through its upregulation induced by the enriched transcription factor HOXA10. Meanwhile, *EPYC* + *HAPLN1*+ fibroblasts may be the seed cells for chondrocyte formation, which highly expressed

chondrogenic genes of *MATN4* and *SOX9*. Because previous reports performed scRNA-seq on adult spinal tissues, the mesenchymal stem cell subgroup (MSC-GJA1) that may differentiate into osteoblast and the heterogeneity of chondrocytes was revealed (Gan et al., 2021; Yang et al., 2021). To be complementary, our results of scRNA-seq on fetal spine showed the potential key subcluster to form chondrocytes, providing new insight on chondrocyte regeneration. Moreover, a recent study analyzed pig embryos and concluded that *HOXA10*, *EPYC*, and *HAPLN1* were critical for bone formation (Li et al., 2021), confirming that chondrocytes may originate from EPYC + HAPLN1+ fibroblasts.

As a vital part of the CNS for signal transmission in the spine, neurocytes are also abundant in the early period. We found a new developmental trajectory separate from two previously reported trajectories and speculated that *SOX3*, *TH*, and *GPM6A* are the key factors driving this developmental trajectory. Surprisingly, neuron subclusters with the two kinds of origins showed separated trajectories at different periods. In line with the previous report that *TAOK1* was associated with neuronal maturation (van Woerden et al., 2021), we observed that *MAB21L2* + *TAOK1*+ neurons (Neu_1) took the terminal position along the developmental trajectory. MEIS2 may be an essential target to promote the early differentiation of neurons originating directly from neural progenitor cells. Based on cell-cell interaction analysis, we confirmed the importance of macrophages during spine development. Additionally, we found that NRP2_SEMA3C may be a driving force attracting macrophages to the spine and that CD74_APP may be the means by which macrophages promote neuronal subcluster development and exert heterogeneity. In future studies, work including searching *EPYC* + *HAPLN1*+ fibroblasts (Fib_12) in the mouse embryos by scRNA-seq can be done to verify the origin of chondrocytes. It will be interesting to verify this hypothesis and explore the relationship between cellular interactions and the transcriptional networks that contribute to spine development.

Limitations of the study

Our work provides a blueprint for understanding human spinal development in the early and midgestational stages at single-cell resolution. Owing to limited access of fetal spine, the number of donors at each age was less than three. Given the small sample size and heterogeneity, the percentage of cells may fluctuate erratically in samples of similar age. Therefore, the difference in developmental time/lineage may be in biological replicate. But in our case, the percentages of fibroblasts, neurocytes, and chondrocytes ranging from 8 to 17 gestational weeks were consistent with previous literature (Zhang et al., 2017b) (Szpinda et al., 2013), indicating the robustness of the scRNA-seq method and the reference value of cellular heterogeneity and developmental lineage by scRNA-seq analysis. Because spines ranging from 8 to 11 gestational weeks were cut into pieces and digested into single cells directly, the spatial distribution of cells remains unclear. In the future, performing spatial transcriptomics experiments will help map cells to their distributions, validate cellular communication, and explain cellular function. Furthermore, scRNA-seq analysis of mouse embryonic spines is critical to validate our scRNA-seq results on fetal spines. Additionally, Cre/loxP-based lineage tracing experiments can be performed to verify that chondrocytes are derived from EPYC + HAPLN1+ fibroblasts (Fib_12) if funding allows.

STAR★METHODS

Detailed methods are provided in the online version of this paper and include the following:

- KEY RESOURCES TABLE
- RESOURCE AVAILABILITY
  - Lead contact
  - Materials availability
  - Data and code availability
- EXPERIMENTAL MODEL AND SUBJECT DETAILS
- METHOD DETAILS
  - Sample collection and processing
  - Tissue dissociation and single-cell suspension preparation
  - scRNA-seq
  - scATAC-seq
  - scRNA-seq quantification and statistical analysis
  - Trajectory analysis
  - Pathway enrichment analysis

- Cell interaction analysis
- Single-cell entropy analysis
- scATAC-seq data filter
- Cluster and annotation
- Gene activity score and coaccessibility analysis
- Multiplexed immunofluorescence

- QUANTIFICATION AND STATISTICAL ANALYSIS

SUPPLEMENTAL INFORMATION

Supplemental information can be found online at https://doi.org/10.1016/j.isci.2022.104679.

ACKNOWLEDGMENTS

This work was Supported by Science and Technology Planning Project of Guangdong Province, China (No. 2021A1515111071 and Guangdong Provincial Clinical Research Center for Birth Defects, No. 2017B 020209001).

AUTHOR CONTRIBUTIONS

Y.D. and Y.Y. conceived the study. M.O. and D.T. designed the experiments. Samples were collected and isolated by D.T., C.L., W.S., W.H., and Z.Z., and the single-cell experiments were performed by F.H. Immunohistochemistry was performed and interpreted by H.Y., and M.O., X.Z., and C.L. generated scRNA-seq datasets and performed the computational analysis. H.Y., M.O., H.W., D.T., and Y.L. interpreted the data. H.Y., M.O., and F.H. wrote the manuscript. Y.D. and W.D. reviewed and improved the manuscript. All authors read and accepted the manuscript.

DECLARATION OF INTERESTS

The authors declare no competing interests.

Received: January 21, 2022
Revised: May 18, 2022
Accepted: June 23, 2022
Published: July 15, 2022

REFERENCES

Alkhatib, B., Ban, G.I., Williams, S., and Serra, R. (2018). IVD Development: nucleus pulposus development and sclerotome specification. Curr. Mol. Biol. Rep. *4*, 132–141. https://doi.org/10.1007/s40610-018-0100-3.

Alonso-Martin, S., Rochat, A., Mademtzoglou, D., Morais, J., de Reyniès, A., Auradé, F., Chang, T.H., Zammit, P.S., and Relaix, F. (2016). Gene expression profiling of muscle stem cells identifies novel regulators of postnatal myogenesis. Front. Cell Dev. Biol. *4*, 58.

Cai, S., Tsui, Y.P., Tam, K.W., Shea, G.K.H., Chang, R.S.K., Ao, Q., Shum, D.K.Y., and Chan, Y.S. (2017). Directed differentiation of human bone marrow stromal cells to fate-committed Schwann cells. Stem Cell Rep. *9*, 1097–1108. https://doi.org/10.1016/j.stemcr.2017.08.004.

Castillo, E., Leon, J., Mazzei, G., Abolhassani, N., Haruyama, N., Saito, T., Saido, T., Hokama, M., Iwaki, T., Ohara, T., et al. (2017). Comparative profiling of cortical gene expression in Alzheimer's disease patients and mouse models demonstrates a link between amyloidosis and neuroinflammation. Sci. Rep. *7*, 17762. https://doi.org/10.1038/s41598-017-17999-3.

Chen, S., Tisch, N., Kegel, M., Yerbes, R., Hermann, R., Hudalla, H., Zuliani, C., Gülcüler, G.S., Zwadlo, K., von Engelhardt, J., et al. (2017). CNS macrophages control neurovascular development via CD95L. Cell Rep. *19*, 1378–1393. https://doi.org/10.1016/j.celrep.2017.04.056.

Curreli, S., Wong, B.S., Latinovic, O., Konstantopoulos, K., and Stamatos, N.M. (2016). Class 3 semaphorins induce F-actin reorganization in human dendritic cells: role in cell migration. J. Leukoc. Biol. *100*, 1323–1334. https://doi.org/10.1189/jlb.2a1114-534r.

Dehne, T., Schenk, R., Perka, C., Morawietz, L., Pruss, A., Sittinger, M., Kaps, C., and Ringe, J. (2010). Gene expression profiling of primary human articular chondrocytes in high-density micromasses reveals patterns of recovery, maintenance, re- and dedifferentiation. Gene *462*, 8–17. https://doi.org/10.1016/j.gene.2010.04.006.

Delile, J., Rayon, T., Sagner, A., Melchionda, M., Edwards, A., and Briscoe, J. (2019). Single cell transcriptomics reveals spatial and temporal dynamics of gene expression in the developing mouse spinal cord. Development *146*, dev173807.

Efremova, M., Vento-Tormo, M., Teichmann, S.A., and Vento-Tormo, R. (2020). CellPhoneDB: inferring cell-cell communication from combined expression of multi-subunit ligand-receptor complexes. Nat. Protoc. *15*, 1484–1506. https://doi.org/10.1038/s41596-020-0292-x.

Furuno, T., Hagiyama, M., Sekimura, M., Okamoto, K., Suzuki, R., Ito, A., Hirashima, N., and Nakanishi, M. (2012). Cell adhesion molecule 1 (CADM1) on mast cells promotes interaction with dorsal root ganglion neurites by heterophilic binding to nectin-3. J. Neuroimmunol. *250*, 50–58. https://doi.org/10.1016/j.jneuroim.2012.05.016.

Galbusera, F., and Bassani, T. (2019). The Spine: A Strong, Stable, and Flexible Structure with Biomimetics Potential. Biomimetics *4*.

Galbusera, F., and Wilke, H.-J. (2018). Biomechanics of the Spine: Basic Concepts, Spinal Disorders and Treatments (Academic Press).

Gan, Y., He, J., Zhu, J., Xu, Z., Wang, Z., Yan, J., Hu, O., Bai, Z., Chen, L., Xie, Y., et al. (2021). Spatially defined single-cell transcriptional profiling characterizes diverse chondrocyte subtypes and nucleus pulposus progenitors in

human intervertebral discs. Bone Res. *9*, 37. https://doi.org/10.1038/s41413-021-00163-z.

Gu, Y., Lv, F., Xue, M., Chen, K., Cheng, C., Ding, X., Jin, M., Xu, G., Zhang, Y., Wu, Z., et al. (2018). The deubiquitinating enzyme UCHL1 is a favorable prognostic marker in neuroblastoma as it promotes neuronal differentiation. J. Exp. Clin. Cancer Res. *37*, 258. https://doi.org/10.1186/s13046-018-0931-z.

Guo, M., Bao, E.L., Wagner, M., Whitsett, J.A., and Xu, Y. (2017). SLICE: determining cell differentiation and lineage based on single cell entropy. Nucleic Acids Res. *45*, e54. https://doi.org/10.1093/nar/gkw1278.

Gut, P., Komarowska, H., Czarnywojtek, A., Waligórska-Stachura, J., Bączyk, M., Ziemnicka, K., Fischbach, J., Wrotkowska, E., and Ruchała, M. (2015). Familial syndromes associated with neuroendocrine tumours. Contemp. Oncol. *3*, 176–183. https://doi.org/10.5114/wo.2015.52710.

Hérault, A., Binnewies, M., Leong, S., Calero-Nieto, F.J., Zhang, S.Y., Kang, Y.A., Wang, X., Pietras, E.M., Chu, S.H., Barry-Holson, K., et al. (2017). Myeloid progenitor cluster formation drives emergency and leukaemic myelopoiesis. Nature *544*, 53–58. https://doi.org/10.1038/nature21693.

Hernangómez, M., Mestre, L., Correa, F.G., Loría, F., Mecha, M., Iñigo, P.M., Docagne, F., Williams, R.O., Borrell, J., and Guaza, C. (2012). CD200-CD200R1 interaction contributes to neuroprotective effects of anandamide on experimentally induced inflammation. Glia *60*, 1437–1450. https://doi.org/10.1002/glia.22366.

Holt, P.G., and Jones, C.A. (2000). The development of the immune system during pregnancy and early life. Allergy *55*, 688–697. https://doi.org/10.1034/j.1398-9995.2000.00118.x.

Hoshi, K., Amizuka, N., Sakou, T., Kurokawa, T., and Ozawa, H. (1997). Fibroblasts of spinal ligaments pathologically differentiate into chondrocytes induced by recombinant human bone morphogenetic protein-2: morphological examinations for ossification of spinal ligaments. Bone *21*, 155–162. https://doi.org/10.1016/s8756-3282(97)00106-3.

Isgrò, M.A., Bottoni, P., and Scatena, R. (2015). Neuron-specific enolase as a biomarker: biochemical and clinical aspects. Adv. Exp. Med. Biol. *867*, 125–143. https://doi.org/10.1007/978-94-017-7215-0_9.

Kaplan, K.M., Spivak, J.M., and Bendo, J.A. (2005). Embryology of the spine and associated congenital abnormalities. Spine J. *5*, 564–576. https://doi.org/10.1016/j.spinee.2004.10.044.

Kolb, J., Anders-Maurer, M., Müller, T., Hau, A.C., Grebbin, B.M., Kallenborn-Gerhardt, W., Behrends, C., and Schulte, D. (2018). Arginine methylation regulates MEIS2 nuclear localization to promote neuronal differentiation of adult SVZ progenitors. Stem Cell Rep. *10*, 1184–1192. https://doi.org/10.1016/j.stemcr.2018.03.010.

Komori, T. (2019). Regulation of proliferation, differentiation and functions of osteoblasts by Runx2. Int. J. Mol. Sci. *20*, 1694. https://doi.org/10.3390/ijms20071694.

Lawson, L.Y., and Harfe, B.D. (2017). Developmental Mechanisms of Intervertebral Disc and Vertebral Column Formation. Wiley Interdiscip. Rev. Dev. Biol. *6*.

Li, J., Wang, L., Yu, D., Hao, J., Zhang, L., Adeola, A.C., Mao, B., Gao, Y., Wu, S., Zhu, C., et al. (2021). Single-cell RNA sequencing reveals thoracolumbar vertebra heterogeneity and ribgenesis in pigs. Dev. Reprod. Biol. *19*, 423–436. https://doi.org/10.1016/j.gpb.2021.09.008.

Li, Y., Sun, Z., Zhu, Z., Zhang, J., Sun, X., and Xu, H. (2014). PBX3 is overexpressed in gastric cancer and regulates cell proliferation. Tumour Biol. *35*, 4363–4368. https://doi.org/10.1007/s13277-013-1573-6.

Liang, X., Song, M.R., Xu, Z., Lanuza, G.M., Liu, Y., Zhuang, T., Chen, Y., Pfaff, S.L., Evans, S.M., and Sun, Y. (2011). Isl1 is required for multiple aspects of motor neuron development. Mol. Cell. Neurosci. *47*, 215–222. https://doi.org/10.1016/j.mcn.2011.04.007.

Loeser, R.F., and Shanker, G. (2000). Autocrine stimulation by insulin-like growth factor 1 and insulin-like growth factor 2 mediates chondrocyte survival in vitro. Arthritis Rheum. *43*, 1552–1559. https://doi.org/10.1002/1529-0131(200007)43:7<1552::aid-anr20>3.0.co;2-w.

Michibata, H., Okuno, T., Konishi, N., Kyono, K., Wakimoto, K., Aoki, K., Kondo, Y., Takata, K., Kitamura, Y., and Taniguchi, T. (2009). Human GPM6A is associated with differentiation and neuronal migration of neurons derived from human embryonic stem cells. Stem Cell. Dev. *18*, 629–640. https://doi.org/10.1089/scd.2008.0215.

Naciff, J.M., Kaetzel, M.A., Behbehani, M.M., and Dedman, J.R. (1996). Differential expression of annexins I-VI in the rat dorsal root ganglia and spinal cord. J. Comp. Neurol. *368*, 356–370. https://doi.org/10.1002/(sici)1096-9861(19960506)368:3<356::aid-cne3>3.0.co;2-4.

Neuman, T., Keen, A., Knapik, E., Shain, D., Ross, M., Nornes, H.O., and Zuber, M.X. (1993). ME1 and GE1: basic helix-loop-helix transcription factors expressed at high levels in the developing nervous system and in morphogenetically active regions. Eur. J. Neurosci. *5*, 311–318. https://doi.org/10.1111/j.1460-9568.1993.tb00498.x.

Nolting, D., Hansen, B.F., Keeling, J., and Kjær, I. (1998). Prenatal development of the normal human vertebral corpora in different segments of the spine. Spine *23*, 2265–2271. https://doi.org/10.1097/00007632-199811010-00003.

Pachynski, R.K., Wang, P., Salazar, N., Zheng, Y., Nease, L., Rosalez, J., Leong, W.I., Virdi, G., Rennier, K., Shin, W.J., et al. (2019). Chemerin suppresses breast cancer growth by recruiting immune effector cells into the tumor microenvironment. Front. Immunol. *10*, 983. https://doi.org/10.3389/fimmu.2019.00983.

Popescu, D.M., Botting, R.A., Stephenson, E., Green, K., Webb, S., Jardine, L., Calderbank, E.F., Polanski, K., Goh, I., Efremova, M., et al. (2019). Decoding human fetal liver haematopoiesis. Nature *574*, 365–371. https://doi.org/10.1038/s41586-019-1652-y.

Saavedra, A.A., Maclellan, D., and Gray, G.J. (2018). Spina bifida. Can. Urol. Assoc. J. *12*, S3–S9. https://doi.org/10.5489/cuaj.5272.

Sanyas, I., Bozon, M., Moret, F., and Castellani, V. (2012). Motoneuronal Sema3C is essential for setting stereotyped motor tract positioning in limb-derived chemotropic semaphorins. Development *139*, 3633–3643. https://doi.org/10.1242/dev.080051.

Sferra, A., Petrini, S., Bellacchio, E., Nicita, F., Scibelli, F., Dentici, M.L., Alfieri, P., Cestra, G., Bertini, E.S., and Zanni, G. (2020). TUBB variants underlying different phenotypes result in altered vesicle trafficking and microtubule dynamics. Int. J. Mol. Sci. *21*, 1385. https://doi.org/10.3390/ijms21041385.

Slack, J.M.W. (2005). Essential Developmental Biology, 2nd ed..

Solovei, I., Wang, A.S., Thanisch, K., Schmidt, C.S., Krebs, S., Zwerger, M., Cohen, T.V., Devys, D., Foisner, R., Peichl, L., et al. (2013). LBR and lamin A/C sequentially tether peripheral heterochromatin and inversely regulate differentiation. Cell *152*, 584–598. https://doi.org/10.1016/j.cell.2013.01.009.

Soltész, B., Lukács, J., Szilágyi, E., Márton, É., Szilágyi Bónizs, M., Penyige, A., Póka, R., and Nagy, B. (2019). Expression of CD24 in plasma, exosome and ovarian tissue samples of serous ovarian cancer patients. J. Biotechnol. *298*, 16–20. https://doi.org/10.1016/j.jbiotec.2019.03.018.

Su, Y., Wang, Y., Zhou, Y., Zhu, Z., Zhang, Q., Zhang, X., Wang, W., Gu, X., Guo, A., and Wang, Y. (2017). Macrophage migration inhibitory factor activates inflammatory responses of astrocytes through interaction with CD74 receptor. Oncotarget *8*, 2719–2730. https://doi.org/10.18632/oncotarget.13739.

Sun, Y., Dykes, I.M., Liang, X., Eng, S.R., Evans, S.M., and Turner, E.E. (2008). A central role for Islet1 in sensory neuron development linking sensory and spinal gene regulatory programs. Nat. Neurosci. *11*, 1283–1293. https://doi.org/10.1038/nn.2209.

Szpinda, M., Baumgart, M., Szpinda, A., Woźniak, A., and Mila-Kierzenkowska, C. (2013). Cross-sectional study of the neural ossification centers of vertebrae C1-S5 in the human fetus. Surg. Radiol. Anat. *35*, 701–711. https://doi.org/10.1007/s00276-013-1093-5.

van Woerden, G.M., Bos, M., Konink, C., Shur, N.E., Distel, B., Barañano, K., Avagliano Trezza, R., Mahida, S., Chassevent, A., Barañano, K., et al. (2021). TAOK1 is associated with neurodevelopmental disorder and essential for neuronal maturation and cortical development. Hum. Mutat. *42*, 445–459. https://doi.org/10.1002/humu.24176.

Walsh, S., Gösswein, S.S., Rump, A., von der Hagen, M., Hackmann, K., Schröck, E., Di Donato, N., and Kahlert, A.K. (2020). Novel dominant-negative NR2F1 frameshift mutation and a phenotypic expansion of the Bosch-Boonstra-Schaaf optic atrophy syndrome. Eur. J. Med. Genet. *63*, 104019. https://doi.org/10.1016/j.ejmg.2020.104019.

Wang, J.B., Zhang, Z., Li, J.N., Yang, T., Du, S., Cao, R.J., and Cui, S.S. (2020). SPP1 promotes

Schwann cell proliferation and survival through PKCα by binding with CD44 and αvβ3 after peripheral nerve injury. Cell Biosci. *10*, 98. https://doi.org/10.1186/s13578-020-00458-4.

Wang, T.W., Stromberg, G.P., Whitney, J.T., Brower, N.W., Klymkowsky, M.W., and Parent, J.M. (2006). Sox3 expression identifies neural progenitors in persistent neonatal and adult mouse forebrain germinative zones. J. Comp. Neurol. *497*, 88–100. https://doi.org/10.1002/cne.20984.

Wang, X., Choi, J.H., Ding, J., Yang, L., Ngoka, L.C., Lee, E.J., Zha, Y., Mao, L., Jin, B., Ren, M., et al. (2013). HOXC9 directly regulates distinct sets of genes to coordinate diverse cellular processes during neuronal differentiation. BMC Genom. *14*, 830. https://doi.org/10.1186/1471-2164-14-830.

Weiss, H.R., and Moramarco, M. (2016). Congenital scoliosis (Mini-review). Curr. Pediatr. Rev. *12*, 43–47. https://doi.org/10.2174/1573396312666151117121011.

Yang, Y., Yang, M., Shi, D., Chen, K., Zhao, J., He, S., Bai, Y., Shen, P., and Ni, H. (2021). Single-cell RNA Seq reveals cellular landscape-specific characteristics and potential etiologies for adolescent idiopathic scoliosis. JOR Spine *4*, e1184. https://doi.org/10.1002/jsp2.1184.

Zhang, M., Zhang, P., Liu, Y., Lv, L., Zhang, X., Liu, H., and Zhou, Y. (2017a). RSPO3-LGR4 regulates osteogenic differentiation of human adipose-derived stem cells via ERK/FGF signalling. Sci. Rep. *7*, 42841. https://doi.org/10.1038/srep42841.

Zhang, W.H., Li, X.L., Guo, Y., and Zhang, Y. (2017b). Proliferation and osteogenic activity of fibroblasts induced with fibronectin. Braz. J. Med. Biol. Res. *50*, e6272. https://doi.org/10.1590/1414-431x20176272.

Zhao, Y., Tang, F., Lee, D., and Xiong, W.C. (2021). Expression of low level of VPS35-mCherry fusion protein diminishes Vps35 depletion induced neuron terminal differentiation deficits and neurodegenerative pathology, and prevents neonatal death. Int. J. Mol. Sci. *22*, 8394. https://doi.org/10.3390/ijms22168394.

STAR★METHODS

KEY RESOURCES TABLE

REAGENT or RESOURCE	SOURCE	IDENTIFIER
Antibodies		
Anti-NeuN	Abcam	#ab177487
Anti-Neurofilament-M	CST	#A10011-60
Anti-CD163	Abcam	#2838
Anti-CD56	JieHao	#ab182422
Anti-S100A9	Abcam	#CRM-0351
Anti-COL1A	CST	#ab92507
Anti-Fibronectin	CST	#72026
Anti-CD15	MXB	#26836 ab182422
Anti-Aggrecan	Abcam	#MAB-0779
Anti-MATN3	Abcam	#ab186414
Anti-CD74	CST	#ab238893
Anti-APP	CST	#77274
Anti-Neuropilin-2	CST	#29765
Anti-HAPLN1	Abcam	#3366
Anti-SEMA3C	R&D	#181997
Anti-EPYC	Novus	#MAB1728-SP
Anti-MATN4	Novus	#NBP2-33445
Anti-ME1	Novus	#NBP1-77012
Anti-UCHL1	CST	#H00004199-M03
Anti-DAPI	Thermo Fisher	#13179
Biological samples		
Healthy Fetal spine	Shenzhen People's Hospital	n/a
Chemicals, peptides, and recombinant proteins		
Buffer EB	QIAGEN	19086
VAHTS DNA clean Beeds	vazyme	N411-02
1XTE Buffer	Sangon Biotech	B548106-0500
Trypan blue	Bio-RAD	1450013
RNase,DNase,RNA and DNA Away	Beyotime	R0127
1XPBS PH7.4	HyClone/	SH30256.01
HBSS	thermo	14025076
NF water	BeyoPure Ultrapure Water	ST876
Pure ethanol	sigma	E7023-1L
sCelLive™ Tissue Preservation Solution	Singleron Biotechnologies	n/a
sCelLive™ Tissue Dissociation Solution	Singleron Biotechnologies	n/a
GEXSCOPE® red blood cell lysis buffer	Singleron Biotechnologies	n/a
Critical commercial assays		
Singleron GEXSCOPE Single Cell RNAseq Library Kit	Singleron Biotechnologies	1100011
Chromium Single Cell ATAC Reagent Kits User Guide	10x genomics	CG000168 Rev. B

(*Continued on next page*)

Continued

REAGENT or RESOURCE	SOURCE	IDENTIFIER
Deposited data		
Raw and analyzed data	This paper	Genome Sequence Archive of the National Genomics Data Center: HRA002609. https://ngdc.cncb.ac.cn/gsa/ and China National GeneBank (CNGB): CNP0001545. http://db.cngb.org/cnsa/project/CNP0001545_1de9a3b6/reviewlink/
Software and algorithms		
CeleScope	v1.9.0	https://github.com/singleron-RD/CeleScope
STAR	version 020201	http://code.google.com/p/rna-star/
featureCounts	version 1.6.2	http://subread.sourceforge.net
Seurat	v3.1.2	https://satijalab.org/seurat/archive/v3.2/pbmc3k_tutorial.html
Monocle	Monocle2	http://monocle-bio.sourceforge.net/
Slingshot	1.4.0	https://github.com/kstreet13/slingshot
clusterProfiler	3.10.1	http://bioconductor.org/packages/release/bioc/html/clusterProfiler.html
STRINGdb	1.22.0	http://bioconductor.org/packages/release/bioc/html/STRINGdb.html
CellphoneDB		https://github.com/Teichlab/cellphonedb
SLICE	0.99.0	https://github.com/xu-lab/SLICE
SnapATAC	version 1.0.0	https://github.com/r3fang/SnapATAC
MACS2	version 2.1.4	https://software.broadinstitute.org/software/igv/
Homer	v4.11	https://github.com/r3fang/SnapATAC
Cicero	version 1.4.0	https://github.com/r3fang/SnapTools

RESOURCE AVAILABILITY

Lead contact

Further information and requests for resources and reagents should be directed to and will be fulfilled by the lead contact, Yong Dai (daiyong22@aliyun.com).

Materials availability

This study did not generate new unique reagents.

Data and code availability

The datasets/code generated during this study are available at both the Genome Sequence Archive of the National Genomics Data Center: HRA002609 (https://ngdc.cncb.ac.cn/gsa/) and the China National GeneBank (CNGB): CNP0001545 (http://db.cngb.org/cnsa/project/CNP0001545_1de9a3b6/reviewlink/).

Any additional information required to reanalyze the data reported in this paper is available from the lead contact upon request.

EXPERIMENTAL MODEL AND SUBJECT DETAILS

We obtained six developmental fetal spine tissue samples from six donors in Shenzhen People's Hospital. The age of fetuses ranges from 53 to 119 days (Table S1). All donors signed informed consent. This work was approved by the ethics committee of Shenzhen People's Hospital (LL-KY-2019591).

METHOD DETAILS

Sample collection and processing

The Ethics Committee approved the human embryo collection and research protocols of Shenzhen People's Hospital (LL-KY-2019591). The six developmental fetal spine tissue samples from six donors ranging from 8 to 17 gestational weeks were collected after the donors signed an informed consent document in strict observance of the legal and institutional ethical regulations for collection of specimens from elective pregnancy termination at Shenzhen People's Hospital. All of the protocols in this study complied with the Interim Measures for the Administration of Human Genetic Resources administered by the Ministry of Science and Technology of China. The tissue samples were processed immediately after isolation (Table S1). Each spine was washed with cold and sterilized PBS twice. After dissection into pieces less than 0.6 cm^3, the spine segments were washed with cold and sterilized PBS twice again and transferred to a 50-ml conical tube containing GEXSCOPE Tissue Preservation Solution (Singleron), followed by shipping to the Singleron laboratory on an ice pack.

Tissue dissociation and single-cell suspension preparation

Fresh tissue samples were washed three times with Hanks' balanced salt solution (HBSS) and shred into 1-2 mm pieces. The tissue pieces were then digested in GEXSCOPE Tissue Dissociation Solution (Singleron Biotechnologies) at 37°C for 15 minutes. A 40-micron sterile strainer (Falcon) was used to separate the cells from cell debris and other impurities. The filtered cells were centrifuged, and the cell pellets were resuspended in PBS (HyClone). GEXSCOPE Red Blood Cell Lysis Buffer (Singleron Biotechnologies) was added to the cell suspension to remove the red blood cells. The mixture was then centrifuged and resuspended in PBS. Cells were counted with a TC20 Automated Cell Counter (Bio-Rad), and the final concentration of the cell suspension was 1×10^5 cells/ml.

scRNA-seq

Single-cell suspensions with a concentration of 1×10^5 cells/ml in PBS were prepared. Single-cell suspensions were then loaded onto microfluidic devices, and scRNA-seq libraries were constructed according to the Singleron GEXSCOPETM protocol by the GEXSCOPETM Single-Cell RNA Library Kit (Singleron Biotechnologies). Individual libraries were diluted to 4 nM and pooled for sequencing. Pools were sequenced on the Illumina HiSeq X platform with 150 bp paired-end reads.

scATAC-seq

ScATAC-seq libraries were prepared according to the Chromium Single Cell ATAC Reagent Kits User Guide (10x Genomics; CG000168 Rev. B). Briefly, the transposition reaction was prepared by mixing the desired number of nuclei with ATAC Buffer (10X Genomics) and ATAC Enzyme (10X Genomics) before incubation for 60 min at 37°C. Indexed sequencing libraries were obtained by mixing the amplification product with Sample Index PCR Mix (10X Genomics) and Chromium i7 Sample Index (10x Genomics). Finally, libraries were loaded on an Illumina HiSeq X with 50 bp paired-end reads.

scRNA-seq quantification and statistical analysis

Gene quantification was performed by featureCounts (version 1.6.2) after aligning the raw reads to the reference genome GRCh38 with Ensembl (version 92) gene annotation software by STAR (version 020201). For high-quality data, cells with 200-5000 genes, less than 30000 UMIs, and a 50% mitochondrial gene expression were selected for the following analysis.

The secondary scRNA-seq data analysis was processed by Seurat (v3.1.2). We used the 2000 highly variable genes to perform principal component analysis (PCA) and used the top 20 principal components for the following cell clustering analysis. Cell clustering was performed by the FindClusters function with a resolution set to 0.8. Finally, we obtained 26 clusters. The FindMarkers function in Seurat with the default parameters was applied to generate differential gene lists of each cluster. The corresponding cell types of the clusters were annotated manually when inspecting the differentially expressed genes. We set the resolution to 1.2 for subclustering fibroblasts, chondrocytes, and neurons. The DoHeatmap function was applied to display the chosen marker genes of each cluster with a heatmap.

Trajectory analysis

According to the five crucial developmental trajectories reported in other studies, we performed Monocle analysis of mesodermal progenitor cells and neuroectodermal progenitor cells. The trajectory was constructed by first choosing the top 2000 highly variable genes found by Seurat and reducing the dimensions by DDRTree. To screen out genes with highly variable expression by pseudotime, the intersection between the 2000 differentially expressed genes found above and the gene set generated by the function differentialGeneTest with qval < 0.001 was selected. These selected differentially expressed genes were clustered into 5 clusters by the function plot_pseudotime_heatmap followed by pathway enrichment analysis.

Furthermore, the R package slingshot (1.4.0) was used to model developmental trajectories after subclustering the neurons because of its ability to handle many branching events arbitrarily. SingleCellExperiment objects were created by a single-cell expression matrix and used as input for slingshot. Based on biological knowledge, neuroectodermal progenitor cells were set as the start of the trajectory when performing the slingshot and getLineages functions.

Pathway enrichment analysis

For GSVA pathway enrichment analysis, the average gene expression of each cell type was used as input data. We selected GO gene sets, which were composed of the molecular function (MF), biological process (BP), and cellular component (CC) categories, as the reference, and the top 30 significant pathways were visualized by a heatmap.

Additionally, we performed GO and Kyoto Encyclopedia of Genes and Genomes (KEGG) enrichment analyses with the clusterProfiler (3.10.1) R package. We regarded pathways with padj < 0.05 as significantly enriched.

According to the protein interaction database STRINGdb (1.22.0), the interactions among differential genes were displayed.

Cell interaction analysis

To study interactions among different cell types or subclusters, CellphoneDB was used to analyze each sample. We set the threshold of cells expressing a gene within each cluster to 0.1 and the iterations to 1000. The interaction with $p < 0.05$ was regarded as significant. The interaction between immune cells was displayed by the circlize (0.4.10) R package.

Single-cell entropy analysis

SLICE (0.99.0) was used to calculate the entropy and stemness based on single-cell expression data. After removing genes starting with 'ERCC' and ribosomal genes, we created a SLICE object and performed a bootstrap calculation of scEntropy to obtain entropy information by the getEntropy function.

scATAC-seq data filter

The scATAC-seq data were aligned to the GRCh38 genome by cellranger-atac (1.2.0). Adapters, low-quality sequences, and repeat sequences were removed, followed by quantification.

Cluster and annotation

The dimension reduction in scATAC-seq data was performed by a diffusion map implemented by SnapATAC software (version 1.0.0). The scATAC-seq data cluster was achieved based on a graph and displayed by Uniform Manifold Approximation and Projection (UMAP). Functional FindTransferAnchors and TransferData in Seurat were used to annotate scATAC clusters based on scRNA-seq data and the predicted results. Those with a score > 0.5 were selected.

After annotation, MACS2 (version 2.1.4) was used for peak calling and to merge peaks of each cluster to generate the cell X peak matrix. The qval threshold of MACS2 was set to 0.05.

SnapATAC was applied to select cell clusters with close distances for comparison and to test the coaccessibility significance by exactTest to obtain each cell type's specific peaks. We obtained motifs by using the

script findMotifsGenome.pl of Homer (v4.11) based on specific peaks, and the script annotatePeaks.pl of Homer completed the peak annotation.

Gene activity score and coaccessibility analysis

The coaccessibility of the peaks was analyzed by the Cicero (version 1.4.0) R package function run_cicero. cellDataSet was created by the cellXpeak sparse matrix, the coaccessibility score was calculated by run_cicero, and results with a coaccessibility score > 0 were selected. Furthermore, Cicero could predict the gene activity and obtain a gene activity score by the function build_gene_activity_matrix based on the relationship among peaks and the location relationship between a peak and gene.

Multiplexed immunofluorescence

Multiplexed immunofluorescence was performed by staining 4-μm-thick formalin-fixed, paraffin-embedded whole tissue sections with standard, primary antibodies sequentially followed by a TSA 7-color kit (D110071-50T, Yuanxibio). Then, the samples were stained with DAPI. For example, deparaffinized slides were incubated with an anti-NeuN antibody (#ab177487 Abcam) for 30 minutes and then treated with an anti-rabbit/mouse horseradish peroxidase-conjugated (HRP) secondary antibody (#A10011-60, Yuanxibio) for 10 minutes. Then, the staining was developed for observation for 10 minutes using TSA 520 per the manufacturer's instructions. Slides were washed in TBST buffer and then transferred to preheated citrate solution (90°C) before being heat-treated in a microwave set at 20% of the maximum power for 15 minutes. Slides were cooled in the same solution to room temperature. Between all steps, the slides were washed with Tris buffer. The same process was repeated for the following antibodies/fluorescent dyes in order: anti-Neurofilament-M (#2838, CST), anti-CD163 (#ab182422, Abcam), anti-CD56 (#CRM-0351, JieHao), anti-S100A9 (#ab92507, Abcam), anti- COL1A1 (#72026, CST), anti-Fibronectin (#26836, CST), anti-CD15 (#MAB-0779, MXB), anti-Aggrecan (#ab186414, Abcam), anti-MATN3 (#ab238893, Abcam), anti-CD74 (#77274, CST), anti-APP (#29765, CST), anti- Neuropilin-2 (#3366, CST), anti-HAPLN1 (#181997, Abcam), anti-SEMA3C (#MAB1728-SP, R&D), anti-EPYC (#NBP2-33445, Novus), anti-MATN4 (#NBP1-77012, Novus), anti-ME1 (#H00004199-M03, Novus), and UCHL1(#13179, CST). Each slide was then treated with two drops of DAPI (D1306; Thermo Fisher), washed in distilled water, and covered with a coverslip. Slides were air-dried, and pictures were taken with the Pannoramic MIDI tissue imaging system (3DHISTECH). A list of primary antibodies including manufacturer and used dilutions was provided in Table S11. Images were analyzed using Indica Halo software.

QUANTIFICATION AND STATISTICAL ANALYSIS

To identify differentially expressed genes (DEGs), we used the Seurat FindMarkers function based on Wilcoxon rank sum test with default parameters, and selected the genes expressed in more than 10% of the cells in both of the compared groups of cells and with an average log(Fold Change) value greater than 0.25 as DEGs. Adjusted p value was calculated by Bonferroni Correction and the value 0.05 was used as the criterion to evaluate the statistical significance.

The statistic significance of differential accessible regions (DARs) was identified using exactTest. Significance was set to pvalue < 0.05 and logFC > 0.